# Development of Gamma-ray Imaging System for Fusion Device Lost Alpha Diagnostics

Doi, Kenta ; Nishiura, Masaki ; Taniike, Akira ; Matsuki, Takuya ; Shimazoe, Kenji ; Mushiake, Toshiki ; Yoshino, Masao ; Kisaki, Masashi…

(Citation)
Journal of maritime researches,5:14-24

(Issue Date)
2015-06

(Resource Type)
departmental bulletin paper

(Version)
Version of Record

(JaLCDOI)
https://doi.org/10.24546/81009084

(URL)
https://hdl.handle.net/20.500.14094/81009084

Journal of Maritime Researches Vol. 5, March 2015: 14-24.

# DEVELOPMENT OF GAMMA-RAY IMAGING SYSTEM FOR FUSION DEVICE LOST ALPHA DIAGNOSTICS

**Kenta DOI***
**Masaki NISHIURA****
**Akira TANIIKE*****
**Takuya MATSUKI******
**Kenji SHIMAZOE*******
**Toshiki MUSHIAKE********
**Masao YOSHINO*********
**Masashi KISAKI**********
**Yoshikatsu MATSUMOTO***********
**Hitoshi YAMAOKA************
**Toshiro KASUYA*************
**Motoi WADA**************

## ABSTRACT

A small-scale simulation experiment based on a tandem accelerator 5SDH2 of Kobe University is being carried out to study the feasibility of the lost alpha diagnostic technique based on gamma-ray imaging. In the experiment, alpha-particles of a given energy simulating lost alphas are directed onto $^{9}$Be target, which is the primary candidate material for the first wall of fusion devices. A Gamma-ray induced by $^{9}Be(\alpha,n\gamma)^{12}C$ reaction at 4.44 MeV energy is detected to construct a two-dimensional image. The imaging system including the scintillator and collimator for the simulation experiment is designed and evaluated by Monte Carlo numerical simulation based on EGS5 code.

**Keywords:** nuclear fusion, lost alpha diagnostics, gamma-ray imaging, ITER

* M.Sc. Student, Graduate School of Science and Engineering, Doshisha Univ., 1-3 Tatara Miyakodani, Kyotanabe-shi, Kyoto, 610-0332, Japan. Email : eup1301@mail4.doshisha.ac.jp
** Associate Professor, Graduate School of Frontier Sciences, The Univ. of Tokyo, 5-1-5 Kashiwanoha, Kashiwa-shi, Chiba, 277-8561, Japan. Email : nishiura@ppl.k.u-tokyo.ac.jp
*** Associate Professor, Graduate School of Maritime Sciences, Kobe Univ., 5-1-1 Fukaeminami-machi, Higashinada-ku, Kobe-shi, Hyogo, 658-0022, Japan. Email : taniike@maritime.kobe-u.ac.jp
**** M.Sc. Student, Graduate School of Maritime Sciences, Kobe Univ., 5-1-1 Fukaeminami-machi, Higashinada-ku, Kobe-shi, Hyogo, 658-0022, Japan. Email : 133w528w@stu.kobe-u.ac.jp
***** Assistant Professor, Department of Bioengineering, The Univ. of Tokyo, 7-3-1 Hongo, Bunkyo-ku, Tokyo, 113-8656, Japan.
Email : shimazoe@it-club.jp

## 1. INTRODUCTION

The efficient operation of a fusion reactor requires comprehensive understanding of the fusion produced alpha-particle behavior in the reactor. Thus, the ITER project takes the introduction of a diagnostic system for fusion produced alphas into account. Deuteron-triton (DT) fusion reaction produces an alpha particle of 3.5 MeV energy, *i.e.*, a fusion produced alpha-particle. In order to keep the fusion energy gain high, it is essential to confine fusion alpha-particles in the core plasma region for the duration that the 3.5 MeV energy is transferred to the fuel plasma (self-ignition). Both simulation and experimental studies, however, have shown that the troidal magnetic field ripple and MHD instabilities can increase the probability of fusion produced alpha losses up to an intolerable level (Zweben 1995; Redi 1996). Losses of fusion alpha-particles can cause not only the deterioration of the self-ignition condition but also damage the first wall as a result of high heat flux irradiation. Thus, a real-time diagnostic system of lost alpha-particles is indispensable for the investigation on ripple-losses and MHD instabilities, which realize the proper plasma control leading to the first wall protection.

Both thermal and neutron radiation make the diagnostics difficult. For ITER operation conditions, the surface heat flux and the average neutron fluence to the first wall are <0.5 MW/m$^2$ and 0.3 MWa/m$^2$, respectively (Bolt 2002; Costley 2005). Under this environment, any detector for alpha-particle measurement, *e.g.* scintillator probe, can hardly be utilized. Nishiura *et al.* (2010) have shown that the lost ion scintillator probe has no resistance to such severe neutron fluence. Table 1 summarizes the features of several lost alpha diagnostic techniques that have been utilized in the previous experiments.

We propose a neutron-resistant lost alpha diagnostic system based on the detection of 4.44 MeV gamma-ray induced by $^9$Be(α,nγ)$^{12}$C reaction. The reaction takes place at the $^9$Be first wall surface by collision with lost alphas with an energy threshold of 1.7 MeV as reported by Kiptily (2004). A fusion produced alpha-particle has the 3.5 MeV energy at its birth. Thus, the positions of lost alpha, *i.e.* the collision points of lost alpha faster than 1.7 MeV, can be specified by imaging the 4.44 MeV gamma-ray originated from the first wall. In this technique, the detectors can be installed relatively far from the core plasma, or with thick neutron shielding reducing noise due to direct neutron radiation to the detector.

**Table 1.** Comparison of features among several lost alpha diagnostic techniques.

| | γ-ray imaging | Scintillator probe | Infrared rays imaging | Activation probe (JET) |
|---|---|---|---|---|
| Measurement target | Loss distribution of fast ions | Pitch angle and energy of lost ions | Thermal loss distribution | Number of lost ions |
| Defect | No corroborative evidence in case of DT plasma | Low radiation resistant | No ability to sort ion species | No time resolution |

## 2. CONCEPT OF GAMMA-RAY IMAGING SYSTEM FOR LOST ALPHA DIAGNOSTICS

The proposed system employs the multi-pixel scintillation gamma-ray detector that observes the first wall to construct an image of lost alpha spatial distribution. The surface of the first wall of the center post side of the torus can be observed directly by the detector mounted on the line extended from the horizontal/equatorial diagnostic port for almost all tokamaks. Figure 1 (a) shows a schematic diagram of the Radial Neutron Camera mounted on the equatorial portplug of ITER (Chugunov 2011; ITER Organization 2009). A similar mounting method can be applied to the gamma-ray detector. On the other hand, the observation of the first wall facing the outer side of the torus plasma through the vertical/upper diagnostic port is impossible due to the observation angle as shown in Figure 1(a). ITER organization has proposed that the port at the lower level can be utilized for the Vertical Neutron Camera mounting position (Fig. 1 (b))(Chugnov 2011; ITER Organization 2009). The gamma-ray detector array for the outer side of the first wall can also have same mounting position (Shevelev 2013). Thus, almost the entire first wall in the poloidal cross-section can be observed.

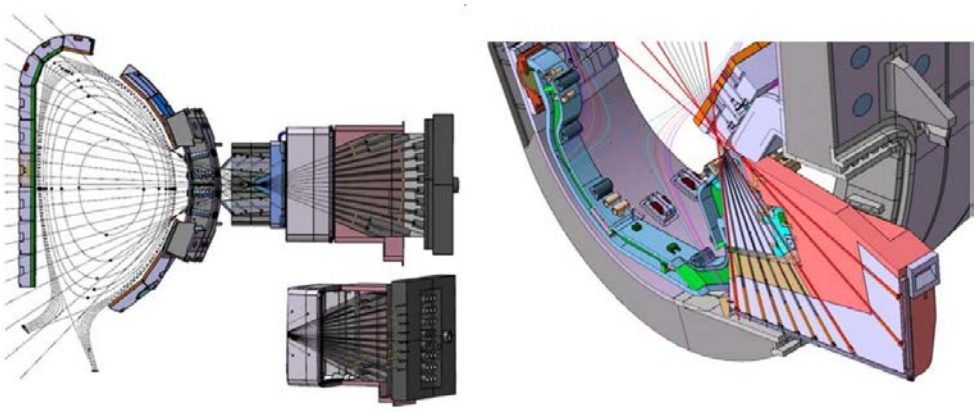

**(a)** Radial Neutron Camera mounted on the equatorial diagnostic port

**(b)** Vertical Neutron Camera mounted on the port at the lower level

**Fig. 1.** Schematic views of ITER neutron camera (Chugunov 2011; ITER Organization 2009).

## 3. DEVELOPMENT OF 4.44 MeV GAMMA-RAY IMAGING SYSTEM

For the development of the gamma-ray imaging system, a small-scale simulation experiment was conducted (Nishiura 2014). A beryllium ($^{9}$Be) target is irradiated with alpha particles accelerated to 1.7 - 3.5 MeV, and the detector obtains the image of 4.44 MeV gamma-ray induced by $^{9}$Be(α,nγ)$^{12}$C reaction. A tandem accelerator 5SDH2 of Kobe University is utilized for the acceleration and irradiation of alpha-particles (Fig. 2). The performance of the detector hardware and the data processing software are examined through the simulation experiment.

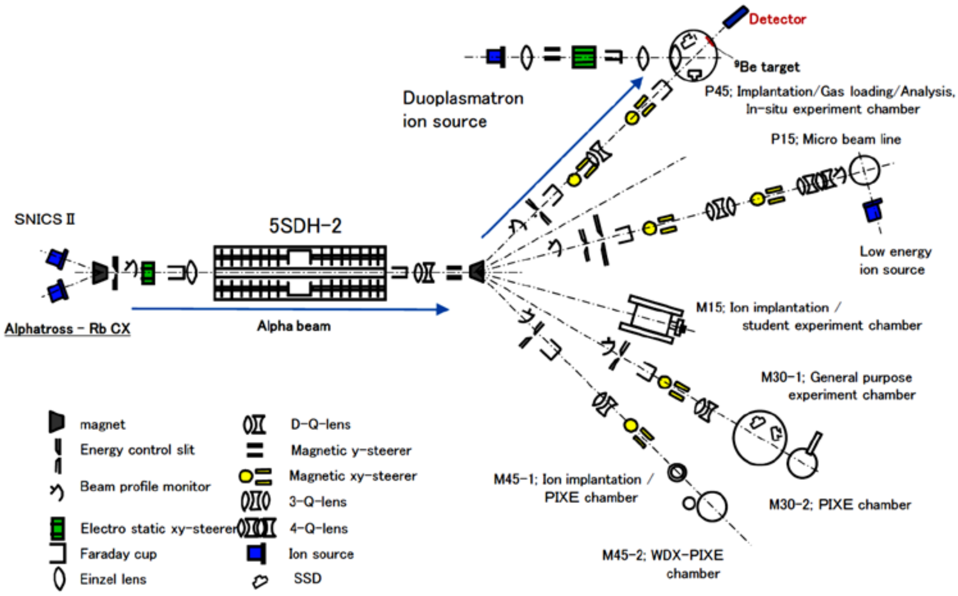


**Fig. 2.** Schematic diagram of the small-scale simulation experiment based on a tandem accelerator 5SDH2, Kobe University. The accelerator makes alpha-particles produced by an ion source Alphatross 1.7 - 3.5 MeV and irradiates a $^{9}$Be target set in the P45 chamber.

## 4. DESIGN STUDY FOR GAMMA-RAY INDUCED ALPHA PARTICLE DIAGNOSTICS

In order to properly design a scintillator and a collimator for the simulation experiment, a Monte Carlo simulation was carried out. The simulation code utilized here is EGS5 (Hirayama 2005). Later sections in this chapter give the details and the results of the simulation.

### 4.1 Numerical Simulation Approaches

#### 4.1.1 Evaluation of GAGG Scintillator Size

The characteristics of several scintillators are listed in Table 2 (Yoshikawa 2013; Furukawa Co., Ltd. -). The scintillator to be used in this study requires high speed response fast enough to clarify the behavior of fusion produced alphas. It also should possess high energy resolution to discriminate lost alpha signals from gamma radiation by other reactions in the fusion environment. The primary candidate scintillation material for this study is Ce:GAGG ($Gd_3Al_2Ga_3O_{12}$:Ce).

To decide the single scintillator area size with the sufficient performance for 4.44 MeV gamma-ray imaging, a simulation of the photon irradiation onto a single scintillator crystal was performed. In this numerical simulation, the center of the incident surface is assumed to be bombarded with a pencil beam of 4.44 MeV photons (Fig. 3). The thickness should be adequately small in order to transmit the scintillator light. Thus, the scintillator thickness is fixed at 47 mm, and the only area size is changed. The area size with the sufficient performance is chosen in accordance with the obtained energy spectrum and detection efficiency.

**Table 2.** Comparison of characteristics among inorganic scintillators (Yoshikawa 2013; Furukawa Co., Ltd. -).

| Crystal | Density ($g/cm^3$) | Decay time (ns) | LY (Ph/MeV) | Energy res. at 662 keV, 5 mm cubic crystal | Self-radiation emission |
|---|---|---|---|---|---|
| Ce:GAGG: | 6.63 | 88 | 46,000-51,000 | 6.3 | no |
| Pr:LuAG | 6.7 | 20 | 16,000-20,000 | 4.2 | yes |
| Ce:LSO | 7.4 | 35 | 26,000 | 9 | yes |
| BGO | 7.13 | 300 | 8,500 | 12 | no |

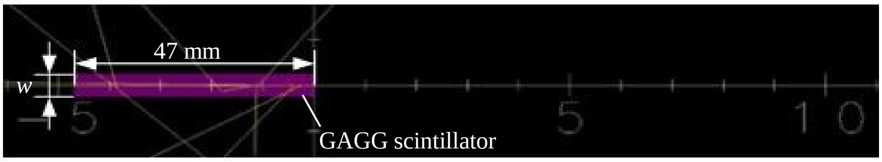


**Fig. 3.** Simulation model and particle trajectories based on Cgview (Namito -). A GAGG scintillator crystal is irradiated with a pencil beam of 4.44 MeV photons.

### 4.1.2 Evaluation of Collimator and Spatial Resolution

A 12×12 pixel parallel array (Fig. 4) similar to a PET detector (Shimazoe 2014) is utilized for the small-scale simulation experiment to reduce the scintillator alignment cost, unlike the fan-shape line of sight as is used in the fusion scale devices. Practically, the parallel alignment of the fan-shape detector array to the toroidal direction is an effective way to obtain the spatial distribution of lost alpha-particles not only in the poloidal cross-section but also in the toroidal direction. But the simple structure is employed here. The collimator designed here is a pinhole-type made of lead suitable to the parallel scintillator array.

The design and dimension of the pinhole collimator is given in Figure 5. The photon sensing side has a square-shaped pinhole and tapered region on the 100 mm thickness lead plate. The visual field is set to make (visual field):(distance from focal point)=1:6. The dimensions $a$ and $b$ also have a correlation as $a$:$b$=1:6 to keep the same angle of observation for different pinhole sizes.

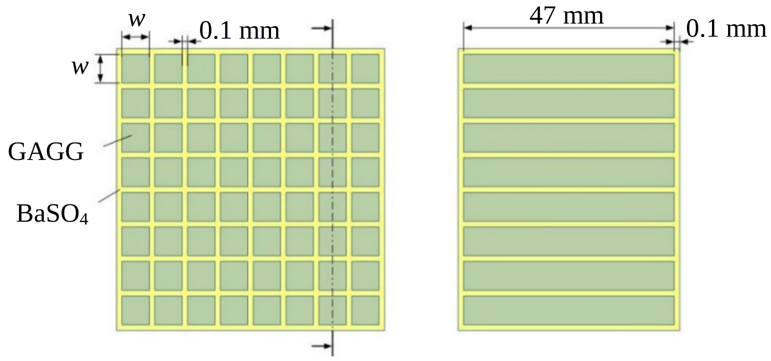


**Fig. 4.** GAGG scintillator array for numerical simulation. Left and right figures are the front and the side views, respectively.

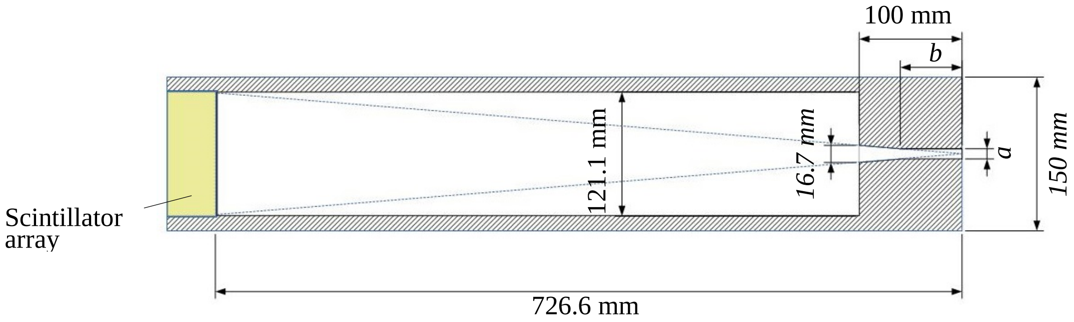


**Fig. 5.** Dimensions of the collimator.

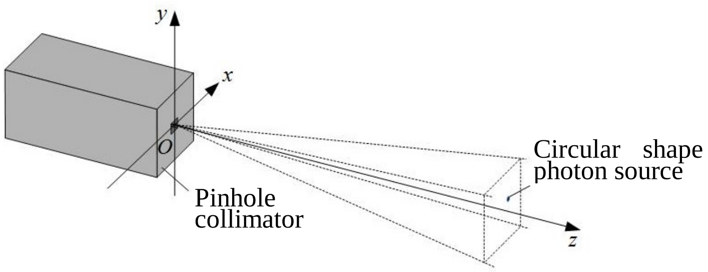


**Fig. 6.** Simulation model of the pinhole collimator made of lead. The collimator is attached to a multi-pixel GAGG scintillation detector. The multi-pixel GAGG scintillator reflects a circular shape source of 4.44 MeV photons passing through the pinhole collimator.

To evaluate the performance including the spatial resolution of the detector consisting of the scintillator array and the collimator mentioned above, gamma-ray images obtained from a circular shape photon source was examined (Fig. 6). The counts of 4.44 MeV full energy (FE) peak in each pixel is stored to the corresponding element of the 12×12 matrix. The emission point and angle on the circular shape source are arbitrarily determined by random numbers.

### 4.2 Numerical Simulation Results

### 4.2.1 Evaluation of Scintillator Size

Figure 7 shows the energy spectra obtained by the numerical simulation in which GAGG scintillators of several sizes are irradiated with 100,000 photons of 4.44 MeV energy. The sizes compared are 2.5×2.5×47 mm, 5.0×5.0×47 mm, 7.5×7.5×47 mm and 10×10×47 mm (width×width×thickness). It was decided that the scintillator for the small-scale simulation experiment was to be 10×10×47 mm although the full energy (FE) peak is still lower than the double escape (DE) peak. The FE, SE and DE counts for 10×10×47 mm GAGG is 4477, 3637 and 6730 per 100,000 incident photons of 4.44 MeV energy, respectively.

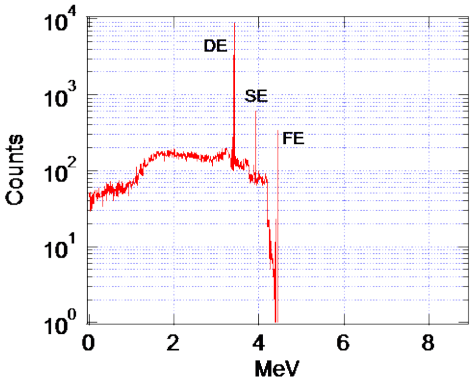


**(a)** 2.5×2.5×47 mm crystal

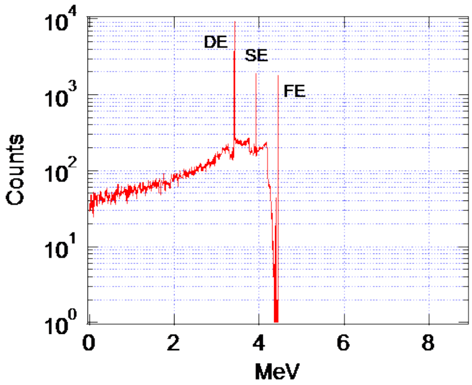


**(b)** 5.0×5.0×47 mm crystal

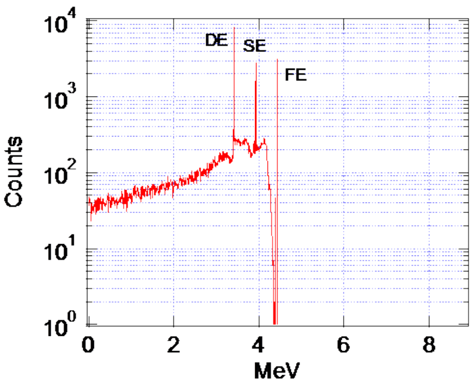


**(c)** 7.5×7.5×47 mm crystal

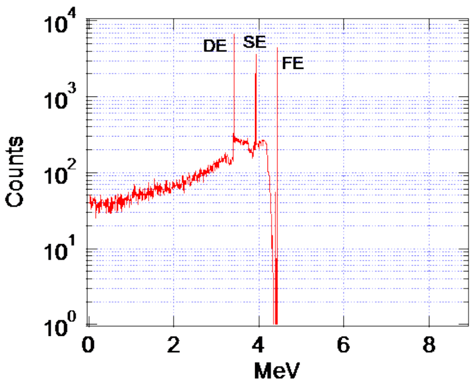


**(d)** 10×10×47 mm crystal

**Fig. 7.** Numerical simulation results of energy spectra for several sizes of GAGG scintillators. The pencil beam of 4.44 MeV photons is assumed to be incident on the center of the scintillator detection surface perpendicular to the 47 mm thickness direction.

### 4.2.2 Evaluation of Collimator and Spatial Resolution

The comparison of the spatial resolution among several side lengths of the square-shaped pinhole collimator was carried out by irradiating the collimator with 4.44 MeV photons from a circular shape source in the numerical simulation. The size of the circular shape photon source was $\varphi$2.0 mm with zero thickness, and its center was positioned at ($x$, *y*, *z*) = (20.8, 20.8, 3000) (mm) as depicted in Fig. 6. It was arranged in parallel to the collimator and the scintillator array surface (*xy* plane), and emitted 10,000,000 photons that hit the collimator surface. From this source position, the image of the photons should appear in one pixel which is located at the sixth position from the left and the bottom since the width of the grid at the circular source position corresponds to the scintillator array at about 41.67 mm. The comparison between the pinhole diameters is 2 to12 mm by 2 mm.

The spatial distributions of 4.44 MeV photons on the scintillator array passing through 2×2 mm and 12×12 mm pinhole collimator are compared in Fig. 8 (a) and Fig. 9 (a) based on the results of the numerical simulation. Figure 8 (b) and Fig. 9 (b) show the 4.44 MeV photon distribution along *x* direction obtained by counting the number of photons in *y* direction as a function of *x*. The FWHM of the distribution along *x* direction for each pinhole dimension compared here is plotted in Fig. 10. The 4×4 mm pinhole collimator has the highest spatial resolution given as 5.1 mm FWHM. Since the area size of one pixel is 10×10 mm, however, the spatial resolution as FWHM can be up to 10 mm to close the photon image from the source positioned at (*x*, *y*, *z*) = (20.8, 20.8, 3000) (mm) in the one pixel. A wider pinhole can have higher detection efficiency. Accordingly, the 8×8 mm pinhole collimator is more suitable to keep the spatial resolution and detection efficiency highest. The comparison of images obtained by the scintillator array with the 4×4 mm, 8×8 mm and 12×12 mm pinhole collimator is given in Fig. 11.

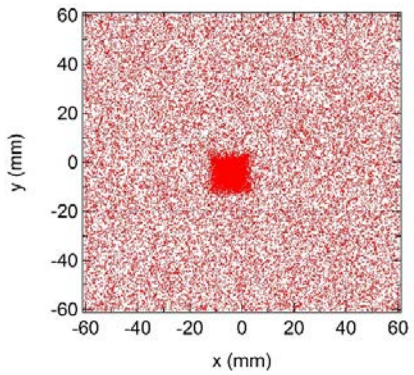


**(a)** Spatial distribution of 4.44 MeV incident photons onto the scintillator array (2×2 mm pinhole collimator)

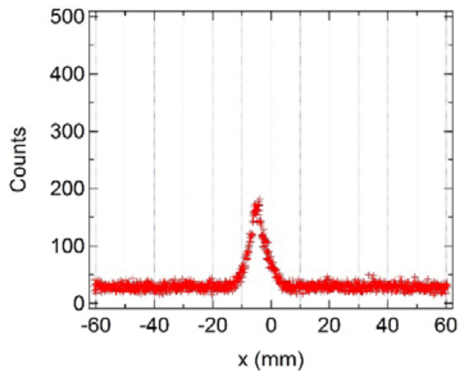


**(b)** 4.44 MeV photon distribution on the scintillator array surface in the *x* direction (2×2 mm pinhole collimator)

**Fig. 8.** Spatial distribution of 4.44 MeV photons on the scintillator array passing through 2×2 mm pinhole collimator (obtained by numerical simulation).

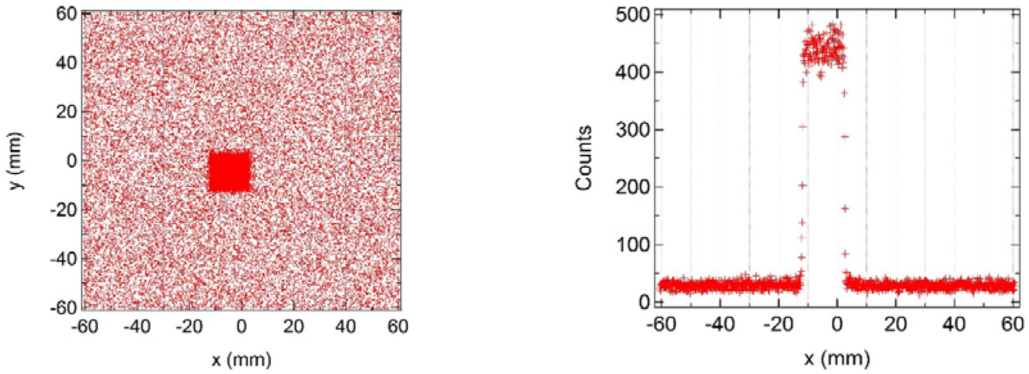


**(a)** Spatial distribution of 4.44 MeV incident photons onto the scintillator array (12×12 mm pinhole collimator)

**(b)** 4.44 MeV photon distribution on the scintillator array surface in the *x* direction (12×12 mm pinhole collimator)

**Fig. 9.** Spatial distribution of 4.44 MeV photons on the scintillator array passing through 12×12 mm pinhole collimator (obtained by numerical simulation).

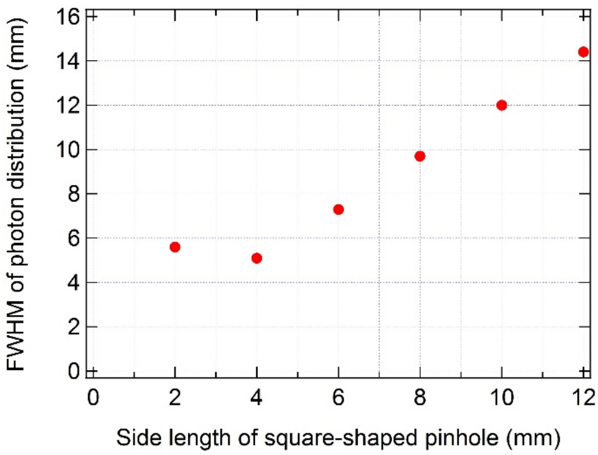


**Fig. 10.** Spatial resolution (FWHM) vs. side length of square-shaped pinhole. The vertical axis gives FWHM of the 4.44 MeV photon spatial distribution on the scintillator surface.

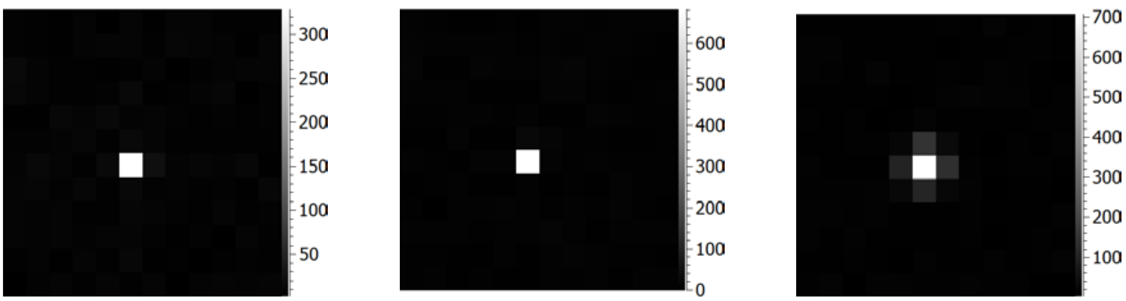

**(a)** 4×4 mm pinhole **(b)** 8×8 mm pinhole **(c)** 12×12 mm pinhole

**Fig. 11.** Image of numerical simulation results for several pinhole collimator dimensions.

## 5. SUMMARY

This paper presented the concept of the lost alpha diagnostics based on imaging 4.44 MeV gamma-ray induced by $^{9}$Be(α, nγ)$^{12}$C reaction. Currently, a small-scale simulation experiment using an accelerator is being conducted to optimize the gamma-ray imaging detector. The gamma-ray detector for the experiment consists of a 12×12 pixel scintillator array and a pinhole made of lead. To decide the scintillator size and collimator dimension with sufficient performance for 4.44 MeV gamma-ray imaging, Monte Carlo calculations based on EGS5 code were carried out. As a result, the scintillator size was determined to be 10×10×47 mm (width×width×thickness), and a pinhole collimator suitable to the scintillator array was evaluated. The visual field was set to 1:6 (visual field : distance from focal point). The gamma-ray imaging setup designed in this paper can theoretically retrieve an image with 8.3 % spatial resolution to the visual field, which is derived as 1:12 (number of pixels for photon image : number of all pixels in *x* direction).

## ACKNOWLEDGEMENT

This work was supported by JSPS KAKENHI Grant No. 24360384 and 25630423.

## REFERENCES

Bolt H., V. Barabash, G. Federici, *et al*. (2002) Plasma facing and high flux materials – needs for ITER and beyond, *J. Nucl. Mater.* 307-311:43-52

Chugunov I.N., A.E. Shevelev, D.B. Gin, *et al*. (2011) Development of gamma-ray diagnostics for ITER, *Nucl. Fusion* 51 (8): 083010-083017.

Costley A.E., T. Sugie, G. Vayakis and C.I. Walker. (2005) Technological challenges of ITER diagnostics, *Fusion Eng. Des.* 74: 109-119.

Furukawa Co. Ltd. (-) Comparison of characteristics among several scintillator crystals (in Japanese), < http://www.furukawakk.co.jp/pdf/others/hikaku.pdf>

Hirayama H. and Y. Namito. (2005) The EGS5 code system, *SLAC-R-730 and KEK Report*, 2005-8.

ITER Organization. (2009) Diagnostics (2WBD7N), *Plant description 2009*, PD: 408-455.

Kiptily V.G., Yu.F. Baranov, R. Barnsley, *et al*. (2004) First gamma-ray measurements of fusion alpha particles in JET trace tritium experiment, *Phys. Rev. Lett.* 93, 115001: 1-4.

Namito Y. and H. Hirayama. (-) CGVIEW – Particle trajectory and geometry display program, <http://rcwww.kek.jp/research/egs/kek/cgview/>

Nishiura M., T. Nagasaka, K. Fujioka, *et al*. (2010) Development and irradiation test of lost alpha detection system for ITER, *Rev. Sci. Instrum.* 81, 10D313: 1-5.

Nishiura M., K. Doi, A. Taniike, *et al.* (2014) Ion-induced gamma-ray detection of fast ions escaping from fusion plasmas, *Rev. Sci. Instrum.* 85, 11E804: 1-3.

Redi M.H., R.V. Budny, D.C. McCune, *et al*. (1996) Simulations of alpha particle ripple loss from the International Thermonuclear Experimental Reactor, *Phys. Plasmas* 3 (8): 3037-3042.

Shevelev A., I. Chugunov, V.G. kiptily, *et al*. (2013) Reconstruction of distribution functions of fast ions and runaway electrons in ITER plasmas using gamma-ray spectrometry, *Nucl. Fusion* 53 (12): 123004-123011.

Shimazoe K., H. Takahashi, K. Kamada, *et al*. (2014) Development of a prototype of time-over-threshold based small animal PET scanner, *J. Nucl. Instr. Meth. Phys. Res. A* 753: 84-90.

Yoshikawa A., V. Chani and M. Nikl. (2013) Czochralski growth and properties of scintillating crystals, *Acta Phys. Pol. A* 124: 250-264.

Zweben S.J., D.S. Darrow, H.W. Herrman, *et al*. (1995) Alpha particle loss in the TFTR DT experiments, *Nucl. Fusion* 35 (8): 893-917.